Detection of T2 changes in an early mouse brain tumor

Blasiak, Barbara; Tomanek, Boguslaw; Abulrob, Abedelnasser; Iqbal, Umar; Stanimirovic, Danica; Albaghhadi, Homam; Foniok, Tadeusz; Lun, Xueqing; Forsyth, Peter; Sutherland, Garnette R.

Publisher's version / Version de l'éditeur:
https://doi.org/10.1016/j.mri.2010.03.004
Magnetic Resonance Imaging, 28, 6, pp. 784-789, 2010-04-15

Detection of T_2 changes in an early mouse brain tumor

Blasiak, Barbara; Tomanek, Boguslaw; Abedelnasser, Abulrob; Iqbal, Umar; Stanimirovic, Danica; Albaghhadi, Homam; Foniok, Tadeusz; Lun, Xueqing; Forsyth, Peter; Sutherland, Garnette R.

Abstract

The aim of the study was to determine the effect of early tumor growth on T_2 relaxation times in an experimental glioma model. A 9.4-T magnetic resonance imaging (MRI) system was used for the investigations. An animal model (*n*=12) of glioma was established using an intracranial inoculation of U87MGdEGFRvIII cells. The imaging studies were performed from Day 10 through Day 13 following tumor inoculation. Tumor blood vessel density was determined using quantitative immunochemistry. Tumor volume was measured daily using MR images. T_2 values of the tumor were measured in five areas across the tumor and calculated using a single exponential fitting of the echo train. The measurements on Days 10 and 13 after tumor inoculation showed a 20% increase in T_2. The changes in T_2 correlated with the size of the tumor. Statistically significant differences in T_2 values were observed between the edge of the tumor and the brain tissue on Days 11, 12 and 13 (*P*=.014, .008, .001, respectively), but not on Day 10 (*P*=.364). The results show that T_2-weighted MRI may not detect glioma during an early phase of growth. T_2 increases in growing glioma and varies heterogenously across the tumor.

Keywords: MRI; Glioma; Molecular imaging; 9.4 T; Mouse model; Brain cancer

1. Introduction

High-grade glioma is the most common central nervous system (CNS) tumor in adults. These tumors have poorly defined margins and directly invade the adjacent brain parenchyma, making complete surgical resection problematic [1]. Additionally, invasive tumor cells are associated with the initiation of angiogenesis with disruption of the blood–brain barrier due to the release of vasomodulatory cytokines [2]. These factors contribute to a rapid growth of the tumor and likely contribute to tumor recurrence [1]. Whereas patients with low-grade glioma can survive for 7 to 15 years, the diagnosis of high-grade glioma carries a median survival of only 9 months [3].

Despite a number of therapeutic approaches over the past several decades, mean survival has been minimally impacted. This can largely be attributed to late tumor detection, its heterogeneity and variable response to conventional therapies. Therefore, better methods allowing tumor detection at the early stage of its growth would enable faster and potentially more efficient treatment. Furthermore, improvement in tumor detection at the early stage is essential because we still rely on tumor size to determine a patient's response to therapy. Since current diagnosis of glioma is often based on magnetic resonance imaging (MRI), early cancer detection using this method is of particular interest. However, studies of early glioma tumor detection with MRI are lacking.

Conventional MRI methods, including T_1-, T_2-weighted and Gd-enhanced MRI, have been used in glioma diagnosis [4], therapy monitoring [5] and even predicting glioma grades [6]. In particular, T_2 methods are among the most frequently used techniques [7], but the changes in T_2 associated with tumor growth remain poorly understood.

In high-grade glioma, T_2 enhancement is associated with retention of plasma fluid and protein in the extracellular space [8] together with infiltrating tumor cells [9]. Furthermore, overexpression of CXCR4, a chemokine receptor known to mediate glioma cell invasiveness, correlates with T_2 signal abnormality [10].

A study with multi-photon fluorescence microscopy [11] demonstrated that tumor growth involves the development of both tumor cells and tumor blood vessels. Tumor vascular density is a prognostic indicator in glioma patients [1] and [12]. Neovascularization in glioblastomas is rapid and involves several mechanisms including co-option, intussusception and sprouting angiogenesis [1] and [9]. High-grade glioma angiogenesis results in highly abnormal, tortuous vessels exhibiting increased permeability and vasogenic edema [13].

Recently introduced molecular MRI [14] uses targeted contrast agents comprising superparamagnetic nanoparticles delivered to the specific cell sites by biologically active targeting moieties, such as antibodies. These agents reduce T_2, thus creating a void signal from tumor in MR images [1] and [15]. As targeted contrast agents can increase the specificity of MRI, any changes in T_2 due to the tumor growth alone should be carefully considered in MRI of glioma using T_2 contrast agents. Therefore, in this study, the relationship between T_2, glioma tumor size and vasculature in the early growth was investigated.

2. Methods

2.1. Tumor cell preparation

The U87MGdEGFRvIII cell line, which overexpresses the EGFR type III variant and is highly malignant, was derived from a human tumor known to express high levels of vascular endothelial growth factor (VEGF) and epidermal growth factor receptor (EGFR) [16]. This cell line exhibits enhanced tumor invasiveness in vivo compared to the U87MG parental and U87MG overexpressing the exogenous wild-type EGFR cell lines [17]. The EGFR is highly expressed in approximately 50% of glioblastoma patient samples owing to the gene amplification [18], while the normal brain exhibits low EGFR expression [19].

The cell line for the study was provided by Dr. W.L. Cavenee (Ludwig Institute for Cancer Research, La Jolla, CA, USA). The U87MG implants grow as solid, nonencapsulated spheroidal tumors. The tumor displays a dense vascular network, with many characteristics of glioblastoma vessels [4], including tortuous vessels with abnormal vascular basement membrane and increased permeability. U87MG cells were cultured in DMEM solution supplemented with 10% fetal calf serum and maintained in a humidified 5% CO_2 atmosphere at 37°C. Cells were harvested by trypsinization in ethylenediaminetetraacetic acid/trypsin, washed in phosphate-buffered saline (PBS) and centrifuged three times at 200×*g*. Viability was assessed using a 0.4% trypan blue exclusion test. After cell density was determined, cells were brought into suspension at a final

concentration of 5×10^4/2.5 µl and mixed with 2.5 µl of matrigel for a total volume of 5 µl. Cells were kept on ice until inoculation.

2.2. Tumor model

Twelve CD-1 nude mice (male, 6 weeks old, Charles River, Canada) were anesthetized by intraperitoneal injection of a mixture of ketamine (8–120 mg/kg) and xylazine (6 mg/kg) and placed in a stereotactic head frame. Tumor cells were inoculated using procedures described previously [20]. Briefly, the scalp was shaved and swabbed with iodine and alcohol. The skin was incised and a 0.18-mm-diameter hole was drilled in the skull. Approximately 5×10^4 U87MGdEGFRvIII glioma cells, suspended in a total volume of 5 µl, were injected intracerebrally into the frontal lobe of each mouse with a chromatography syringe at a depth of 2.5–3 mm (1 mm anterior and 1.8 mm lateral to the bregma) using a Kopf stereotactic apparatus (Kopf Instruments, Tujunga, CA, USA). Subsequently, the bony calvarium was sealed by a droplet of bone wax to prevent reflux and the skin was sutured. After the surgery, animals were allowed to recover from the anesthesia and were placed in the cages. Mice were euthanized on Day 14 with pentobarbital (120 mg/kg iv). The animal procedures were approved by the University of Calgary and National Research of Canada Animal Care Committees.

2.3. MRI Protocol

The MR imaging sessions started 10 days after cell inoculation. A 9.4-T/21-cm horizontal bore magnet (Magnex, UK) with a Biospec console (Bruker, Germany) was used. Data acquisition was gated with the respiratory cycle. A volume (3 cm diameter, 2.5 cm long) radiofrequency coil was placed over the animal's head covering the region of interest (ROI). T_2 images were acquired from the tumor region. Axial slices were positioned within the tumor. A multislice, multiecho sequence was used with TR=5000 ms, 16 echoes, 10 ms apart each, first echo at 10 ms, FOV=3×3 cm, matrix size of 256×256 and slice thickness of 1 mm. T_2 values of the tumor tissues were measured using a single exponential fitting of the echo train from ROIs (Marevisi, NRC, Canada). T_2 values were calculated in five areas across the tumor (Fig. 1): in the center of the tumor (Point C), at its edge (Points A and E), in two points around the center (Points B and D) and outside the tumor (Point Y). Each area comprised 4 pixels. The volume of the tumor was calculated using MRI by measuring the area of each slice and multiplied by slice thickness and adding the results over the entire tumor volume.

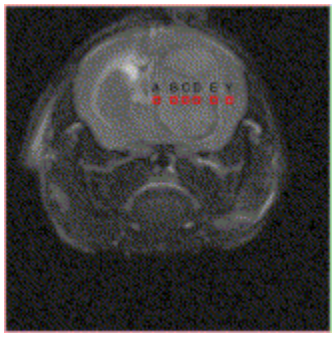

Fig. 1.

An example of a T_2-weighted MRI (spin echo, TR/TE=5000/60 ms) 12 days after inoculation. T_2 values were derived from each area marked as A, B, C, D, E and Y. A and E correspond to edge of the tumor; C, the center of the tumor; B and D, the middle area the tumor; Y, area outside the tumor.

2.4. Hematoxylin and eosin staining of brain tumor sections

Four sections (n=4) from four animals were used for analysis on Day 10 and Day 13 after inoculation. Mice were sacrificed via intracardiac perfusion using deep anesthesia. The animals were perfused with heparinized saline, their brain dissected and then frozen on dry ice. Mouse brains were embedded in Tissue-Tek freezing medium (Miles Laboratories, Elkhart, IN, USA) and sectioned with a cryostat (Jung CM3000; Leica, Richmond Hill, ON, Canada) at 10 μm thickness, then mounted on Superfrost Plus microscope slides (Fisher Scientific, Nepean, ON, Canada). Slides were stored at −80°C until analysis. Frozen brain tumor tissue sections were thawed for a few seconds then incubated in methanol for 10 min at room temperature (RT). The sections were washed in a tray with distilled water. Mayer's hematoxylin solution was added directly to the section (0.1% hematoxylin, 5% alum, 0.02% sodium iodate, 0.1% citric acid) for 5 min. The sections were then washed three times with distilled water. Bluing reagent (0.1% sodium bicarbonate) was added directly to the section for 1 min. Sections were quickly washed in distilled water, and 1% Eosin Y was added directly to the section for 2 min. Eosin Y was washed off with distilled water three times, and sections were coverslipped with mounting media and observed under a color camera (BX-50 Olympus research microscope, with a Color5 camera, Centre Valley, PA, USA).

2.5. Immunohistochemistry of brain tumor sections

After sectioning and fixing sections in methanol as described above, slides were rinsed with 0.2 M PBS (pH 7.3), followed by incubation with 5% donkey serum in PBS for 1 h with 0.1% triton-X 100 at RT. After blocking, slides were incubated with rat anti-mouse CD31 primary antibody (1:300) for 1 h at RT. Slides were then washed with PBS three times, before incubation with a secondary antibody, goat-anti-rat alexa 568 (1:500), for 1 h at RT. A control slide without incubation with the CD31 primary antibody was also made (data not shown). Following this procedure, slides were washed with PBS five times, dried of excess liquid and then coverslips were mounted using DAKO fluorescent mounting media containing Hoechst 33342 (10 μl/μl, Invitrogen, Burlington, ON, Canada) and visualized under fluorescent microscope (Olympus 1X81, Markham, ON, Canada). InVivo and ImagePro 6.2 software packages were used to measure the area of vessels per unit (mm^2) area (vessel density). CD31-positive staining was applied. We measured the vessel density because it allows accurate measurements of angiogenesis including sprouting, intercalated and intussusceptive growth [21].

2.6. Data analysis

To analyze the differences in T_2 values in each measured area, a one-way variance analysis using SigmaStat (USA) and a Student–Newman–Keul's comparison of means were used. The quantification of brain blood vessels was performed as described previously. The tumor mass was first identified using Hoechst 33342 staining of cell nuclei, followed by the analysis of vessels inside an area of interest containing the tumor. The data are presented as the mean±standard deviation of the mean. The difference between Day 10 and Day 13 in tumor bearing mice was analyzed using a Student's *t* test (GraphPad Prism 4.0, USA). The differences in T_2 with a *P* value ≤.05 were considered to be statistically significant.

3. Results

3.1. Magnetic resonance imaging

MR images of glioma were obtained beginning on Day 10 after cell inoculation (Fig. 2). At this time, the tumor was large enough (1.2 to 2.9 mm^3±0.3) to be detected with MRI.

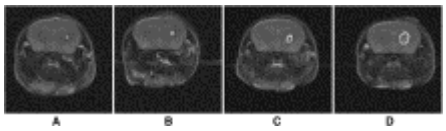

Fig. 2.

Axial MR images (spin echo, TR/TE= 5000/60 ms) of glioma obtained from the same mouse on Days 10 (A), 11 (B), 12 (C) and 13 (D) after tumor inoculation.

A linear increase of the tumor volume from Day 10 to Day 13 was observed (Fig. 3). A significant correlation (*P*≤.001) between tumor size and its T_2 relaxation time (Fig. 4) was detected. High-quality T_2-weighted MR images on Day 12 after cell inoculation allowed detection of different regions of the tumor (Fig. 1). The T_2 values were calculated for each region separately and their corresponding T_2 values are shown in Fig. 5. The results show statistically significant difference in T_2 values between the edge of the tumor (A and E in Fig. 1) and the brain (Y in Fig. 1) on Days 11, 12 and 13 (*P*=.014, .008, .001, respectively), but not on Day 10 (*P*=.364). Significant differences in T_2 between the tumor (B–D in Fig. 1) and brain areas (Y in Fig. 1) were observed on Days 11, 12 and 13 after inoculation. T_2 was uniform across the tumor area (B–D in Fig. 1) on Days 10, 11 and 12. T_2 in the center of the tumor (C in Fig. 1) was not significantly different (*P*=.59) than T_2 outside of the tumor center (E in Fig. 1) on Day 13. The results also show a statistically significant difference between the center of the tumor (C in Fig. 1) and the brain (Y in Fig. 1) on all days.

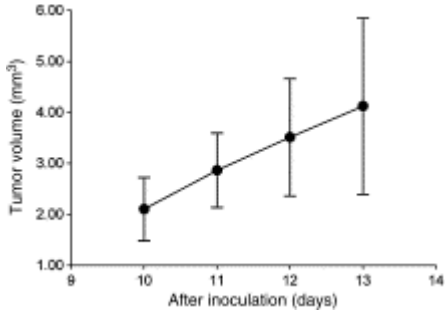

Fig. 3.

Tumor volume measured 10, 11, 12 and 13 days after tumor inoculation using MRI. The data are collected from 12 animals and averaged.

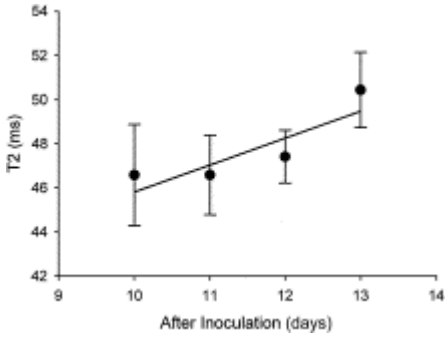

Fig. 4.

T_2 relaxation times measured from the entire area of the tumor 10, 11, 12 and 13 days after tumor inoculation. The data are collected from 12 animals and averaged. Bars indicate standard deviation of the mean.

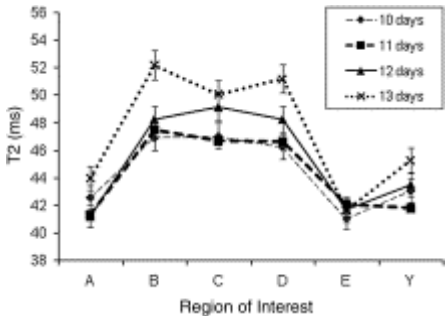

Full-size image (34K)

Fig. 5.

T_2 relaxation times of the tumor regions corresponding to Fig. 4: ♦, ▪, ▲, × indicate Days 10, 11, 12 and 13 after tumor inoculation, respectively.

3.2. Intratumoral vessel density measurements

U87MG deltaEGFRvIII brain tumors grew in a spherical shape over the course of the experiment (Fig. 6). Hematoxylin and eosin staining (Fig. 6A and B) demonstrated a higher density of cell nuclei for brain tumors compared to normal brain regions. This result was paralleled by fluorescent staining using Hoescht 33342 for cell nuclei (Fig. 6C and D). Endothelial cells were identified by immunohistochemical labeling of tissue sections using a platelet–endothelial cell adhesion molecule (PECAM-1/CD31). Microvessel surfaces were assessed by analysis of CD31-positive vessels in a defined ROI using ImagePro. There was a statistically significant (P<.01) increase in the area of blood vessels per unit area. The vessel surface density increased from 307±41 to 390±45 $\mu m^2/mm^2$ between Day 10 and Day 13 (Fig. 6E and F).

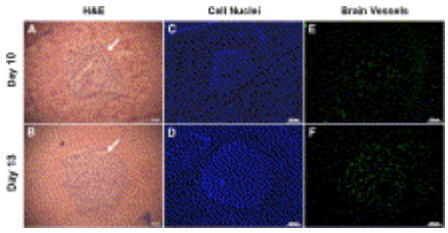

)

Fig. 6.

Brain tumor vessel density in tumor-bearing mice on Days 10 and 13. Brain tumor sections (10 μm) on Days 10 and 13 were stained with Mayer's hematoxylin and eosin (A, B) to visualize the tumor region (white arrow). Immunohistochemistry on Days 10 and 13 of brain tumor sections followed by fluorescent microscopy shows cell nuclei (Hoechst 33342) (C, D) and brain tumor vessels (anti-CD31 antibody) (E, F).

4. Discussion

The T_2 signal abnormalities associated with high-grade glioma are multifactorial in nature. The presence of invading tumor cells and neovascularization is thought to be the most important [22]. The presence of increased T_2-weighted peritumoral signal suggests a worse clinical prognosis in patients with high-grade glioma [23]. Additionally, the elaboration of multiple cytokines by endothelial tumor cells contributes to the generation of vasogenic edema [22]. It was also shown that glioma cell invasiveness and neovascularization are associated with CXCR4 expression [24], while elevated CXCR4 correlates with increased T_2 values in MR images [22]. Glioma is also frequently associated with significant involvement of peritumoral parenchyma as evidenced by the presence of increased T_2 in that region [25] and [26]. Hypervascularization contributes to malignant glioma phenotype by providing oxygenation and nutritional supply needed for tumor growth and supporting the invasion of tumor cells into the surrounding intact brain tissue [27].

High-grade glioma vessels are tortuous and leaky [22]. The tissue shows microvascular hyperplasia, with micro-aggregates of proliferating endothelial cells at the edge of the parental blood vessels [22]. Chronic overproduction of angiogenic factors in tumors leads to uncontrolled development of new blood vessels, increased vascular permeability and a unique phenotype [28]. VEGF has been investigated as a potent mediator of brain tumor angiogenesis, vascular permeability and glioma growth, and is known to be up-regulated in most cases of high-grade glioma [29]. Other angiogenic factors also appear to contribute to the vascularization of high-grade glioma such as bFGF, angiopoietin-1 and angiopoietin-2.

Early detection of neoplasia, when the tumor is less than 1 mm in size, would theoretically be associated with long-term survival [30]. However, conventional anatomical imaging techniques typically detect neoplasia of 1 cm volume or larger (containing about 1 million cells) greatly decreasing survival [31].

Tumor growth and infiltration may differ according to genotype, and these differences may be reflected on MRI. Clinical tumor segmentation requires operator's input and it is based on manual marking of tumor edges on T_2-weighted MRI [22] and [24]. Therefore, the precise determination of the tumor edges is of particular interest and, as shown in the present study, may vary depending on the stage of tumor development.

In small tumors, the existing vascular network in the normal brain is sufficient to provide oxygen and nutrients to the tumor cells. However, for the tumor to expand, it must induce angiogenesis to support continued growth [31]. By initiating angiogenesis, the tumor can induce the host's microvasculature to undergo sprouting, thereby effectively supporting the tumor ability to invade the surrounding parenchyma [32]. It is evident from the result of this study that the tumor vasculature is lar[33].

The present study showed the T_2 increase in the tumor region corresponded with an increase in tumor vessel density. Whether this increase is solely responsible for the increase in T_2 has yet to be determined. The results are important in the early diagnosis of glioma and suggest that the detection limit of a small tumor with MRI is associated with both the small size of the tumor and the small difference in T_2 relaxation times between tumor and normal brain. The results also indicate that molecular MRI, using targeted contrast agents to enhance the detection of a relatively small number of glioma cells, may be problematic as its sensitivity may depend on the stage of tumor development. During the early growth of a tumor, the T_2 value varies with tumor size and age. This needs to be considered in the ongoing development of cell-specific contrast agents [34].

The growth of glioma and aberrant vasculature can affect the ability of MRI to image the tumor. Thus, understanding tumor processes and their corresponding T_2 changes are important in MRI applications and critical in developing effective molecular MRI contrast agents.

References

[1] A. Claes, P. Wesseling and A.J. Idema, Diffuse glioma growth: a guerilla war, *Acta Neuropathol* **114** (2007), pp. 443–458.

[2] A.M. Villalba, A.F. Okuducu and A. Deimling, The evolution of our understanding of glioma, *Brain Pathol* **18** (2008), pp. 455–463.

[3] H. Ohagaki and P. Kleihues, Population based studies on incidence, survival rates, and genetic alterations in astrocytic and oligodendroglial gliomas, *J Neuropathol Exp Neurol* **64** (2005), pp. 479–489.

[4] D.B. Ellegala, H. Leong-Poi and J.E. Carpenter *et al.*, Imaging tumor angiogenesis with contrast ultrasound and microbubbles targeted to $\alpha_v\beta_3$, *Circulation* **108** (3) (2003), pp. 336–341.

[5] F. Fellner, C. Fellner, P. Held and R. Schmitt, Comparison of spin-echo MR pulse sequences for imaging of the brain, *Am J Neuroradiol* **18** (1997), pp. 1617–1625.

[6] M. Aghi, P. Gavani, J.W. Henson, T.T. Batchelor, D.N. Louis and F.G. Barker II, Magnetic resonance imaging characteristics predicts epidermal growth factor receptor amplification status in glioblastomas, *Clin Cancer Res* **11** (24) (2005), pp. 8600–8655.

[7] J. Oh, S. Cha and A.H. Aiken *et al.*, Quantitative apparent diffusion coefficients and T_2 relaxation times in characterizing contrast enhancing brain tumors and regions of peritumoral edema, *J Magn Reson Imag* **21** (2005), pp. 701–708.

[8] H.J. Reulen, R. Graham, M. Spatz and I. Klatzo, Role of pressure gradients and bulk flow in dynamics of vasogenic brain edema, *J Neurosurgery* **46** (1) (1977), pp. 24–35.

[9] J. Strugar, D. Rothbart, W. Harrington and J.R. Criscuolo, Vascular permeability factor in brain metastases correlation with vasogenic brain edema and tumor angiogenesis, *J Neurosurgery* **81** (1994), pp. 560–566.

[10] C.B. Stevenson, M. Ethesham and K.M. McMillan *et al.*, CXCR4 Expression is elevated in glioblastoma multiforme and correlates with an increase in intensity and extend of peritumoral T_2-weighted magnetic resonance imaging signal abnormalities, *Neurosurgery* **63** (3) (2008), pp. 560–569.

[11] G.M. Tozer, S.M. Ameer-Beg and J. Baker *et al.*, Intravital imaging of tumor vascular networks using multi-photon fluorescence microscopy, *Advanced Drug Deliver Reviews* **57** (2005), pp. 135–152.

[12] J. Skong, T. Wurdinger and S. Rijn *et al.*, Glioblastoma microvesicles transport RNA and proteins that promote tumor growth and provide diagnostic biomarkers, *Nat Cell Biol* **10** (12) (2008), pp. 1470–1476.

[13] T. Kuroiwa, R. Cahn, M. Juhler, G. Goping, G. Campbell and I. Klatzo, Role of extracellular proteins in the dynamics of vasogenic brain edema, *Acta Neuropathol* **66** (1985), pp. 3–11.

[14] G.M. Lanza, R. Lamerichs, S. Caruthers and S.A. Wickline, Molecular Imaging in MR with targeted paramagnetic nanoparticles, *MedicaMund* **47** (2003), pp. 34–39.

[15] G. Gambarota, W. Leenders, C. Maass, P. Wesseling, D.B. Tellinge and O. Heerschap, Characterisation of tumor vasculature in mouse brain by USPIO contrast-enhanced MRI, *Br J Cancer* **98** (2008), pp. 1784–1789.

[16] M.M. Nishikawa, O.D. Sant'Anna, M.S. Lazera and B. Wanke, Use of D-proline assimilation and CGB medium for screening Brazilian *Cryptococcus neoformans*, *J Med Vet Mycol* **34** (5) (1996), pp. 365–366.

[17] M. Nagane, S. Shibui, R. Nishikawa, H. Oyama, Y. Nakanishi and K. Nomura, Triple primary malignant neoplasms including a malignant brain tumor: report of two cases and review of the literature, *Surg Neurol* **45** (3) (1996), pp. 219–229.

[18] T.A. Libermann, H.R. Nusbaum and N. Razon *et al.*, Amplification, enhanced expression and possible rearrangement of EGF receptor gene in primary human brain tumours of glial origin, *Nature* **313** (5998) (1985), pp. 144–147.

[19] T.F. Liu, S.B. Tatter, M.C. Willingham, M. Yang, J.J. Hu and A.E. Frankel, Growth factor receptor expression varies among high-grade gliomas and normal brain: epidermal growth factor receptor has excellent properties for interstitial fusion protein therapy, *Mol Cancer Ther* **2** (8) (2003), pp. 783–787.

[20] W. Moller-Hartmann, S. Herninghaus, T. Krings, G. Marquardt and H. Lanfermann, Clinical application of proton magnetic resonance spectroscopy in the diagnosis of intracranial mass lesions, *Neuroradiology* **44** (2002), pp. 371–381.

[21] N.L. Ward, E. Moore and K. Noon *et al.*, Cerebral angiogenic factors, angiogenesis, and physiological response to chronic hypoxia differ among four commonly used mouse strains, *J Appl Physiol* **102** (2007), pp. 1927–1935.

[22] B. Charles, E. Stevenson and M.K. McMillan *et al.*, CXCR4 Expression is elevated in glioblastoma multiforme and correlates with an increase in intensity and extent of peritumoral T2-weighted magnetic resonance imaging signal abnormalities, *Neurosurgery* **63** (2008), pp. 560–569.

[23] M.A. Hammoud, R. Sawaya, W. Shi, P.F. Thall and N.F. Leeds, Prognostic significance of preoperative MRI scan in glioblastoma multiforme, *J Neurooncol* **27** (1996), pp. 65–73.

[24] M. Ehtesham, J.A. Winston, P. Kabos and R.C. Thompson, CXCR4 expression mediates glioma cell invasiveness, *Oncogene* **25** (2006), pp. 2801–2806.

[25] J. Kelly, C. Daumas-Duport, D.B. Kispert, B.A. Kall and B.W. Scheithauer, Imaging-based stereotaxic serial biopsies in untreated intracranial glial neoplasms, *J Neurosurg* **66** (1987), pp. 865–874.

[26] A.M. Villalba, A.F. Okuducu and A. Deimling, The evolution of our understanding on glioma, *Brain Pathol* **18** (2008), pp. 455–463.

[27] P. Vajkoczy, M.D. Menger and B. Vollmar *et al.*, Inhibition of tumor growth, angiogenesis, and microcirculation by the novel Flk-1 inhibitor SU5416 as assessed by intravital multi-fluorescence videomicroscopy, *Neoplasia* **1** (1) (1999), pp. 31–41.

[28] M.D. Jenkinson, D.G. Du Plessis, C. Walker and T.S. Smith, Advanced MRI in the management of adult gliomas, *Br J Neurosurg* **21** (6) (2007), pp. 550–561.

[29] J. Provias, K. Claffey, L. delAguila, N. Lau, M. Feldkamp and A. Guha, Meningiomas: role of vascular endothelial growth factor/vascular permeability factor in angiogenesis and peritumoral edema, *Neurosurgery* **40** (1997), pp. 1016–1026.

[30] R. Etzioni, N. Urban, S. Ramsey, M. McIntosh, S. Schwartz and B. Reid *et al.*, The case for early detection, *Nat Rev Cancer* **3** (4) (2003), pp. 243–252.

[31] J. Folkman, Tumor angiogenesis: therapeutic implications, *N Engl J Med* **285** (1971), pp. 1182–1186.

[32] J. Folkman, Role of angiogenesis in tumor growth and metastasis, *Semin Oncol* **29** (2002), pp. 15–18.

[33] D.R. Groothuis, The blood–brain and blood–tumor barriers: a review of strategies for increasing drug delivery, *Neuro Oncol* **2** (2000), pp. 45–59.

[34] X.H. Peng, X. Qian and H. Mao *et al.*, Targeted magnetic iron oxide nanoparticles for tumor imaging and therapy, *Int J Nanomed* **3** (3) (2008), pp. 311–321.